J. Math. Biol. (1993) 31: 703–716

Journal of
Mathematical
Biology

Actin aggregation and embryonic epidermal wound healing

Jonathan A. Sherratt
Centre for Mathematical Biology, Mathematical Institute, 24–29 St. Giles', Oxford OX1 3LB, UK

Received 30 July 1991; received in revised form 6 August 1992

Abstract. Recent experiments on the response of embryonic epidermis to wounding have revealed a cable of filamentous actin at the wound edge, which may be responsible for healing (Martin and Lewis 1991, 1992). We investigate the important question of how the cable forms as a response to wounding. We modify the mechanical model of Murray and Oster (1984) to investigate the post-wounding equilibrium in the epidermal sheet. We analyse the model in both one-dimensional and radially symmetric two-dimensional geometries, to determine the parameter domain in which a solution exists. We show that in both geometries the model solutions reflect the phenomenon of the actin cable for parameter values close to one edge of this domain. We interpret these results in terms of the relative rates of intracellular reorganization of actin and myosin, and thus suggest a possible mechanism for the formation of the actin cable.

Key words: Actin cable – Wound healing – Epidermal migration

1 Introduction

Epidermal wounds in adult mammals heal by the spreading of epidermal cells across the exposed mesenchyme (Winter 1962). Although debate continues on many aspects of the process (Stenn and DePalma 1988, Sherratt and Murray 1991, 1992), lamellipodial crawling is now established as the mechanism by which the free edge moves (Clark 1989). In contrast, embryonic epidermal wound healing is very poorly understood, but recent experiments suggest that wound closure may be caused by the contraction of a cable of filamentous actin at the wound edge, without lamellipodial crawling (Martin and Lewis 1991, 1992, Midwinter et al. 1992).

In their study of epidermal migration in four-day chick embryos, Martin and Lewis (1991, 1992) made square lesions on the dorsal surface of the wing buds. At this stage in development, the epidermis is two cell layers thick, consisting of a superficial, pavement-like peridermal layer and a cuboidal basal layer. Although the epidermis moved rapidly across the underlying mesenchyme, there was no evidence of lamellipodia at the wound front in either the basal or peridermal layers. However, staining with fluorescently tagged phalloidin re-

vealed a thick cable of filamentous actin around almost all of the wound margin, localized within the leading row of basal cells, which remained present until the wound was closed. The possibility that wound closure was caused by contraction of this cable, in a 'purse string' mechanism, was supported by the finding that when a small island of skin was grafted onto a denuded region of the limb-bud surface, the transplanted epidermis contracted over its own mesenchyme, rather than expanding over the adjacent exposed mesenchyme.

In this paper, we investigate the formation of the actin cable as a response to injury. A detailed study of linear slash wounds by Midwinter et al. (1992) has revealed that the cable begins to form within a few minutes of wounding. We develop and analyse a simple mechanical model which addresses the possibility that the cable forms by compaction and reorientation of the actin filament network, without either de novo actin polymerization or intracellular movement of intact actin filaments. Our results suggest a possible mechanism for the formation of the actin cable.

2 A simple mechanical model

We model the initial response of the basal cell sheet to wounding by modifying the mechanochemical model for the deformation of epithelial sheets proposed by Murray and Oster (1984). This was the first continuum mechanochemical model for epithelial morphogenesis, and was based on the discrete model of Odell et al. (1981); Murray (1989) gives an in depth review of mechanical models for morphogenesis. The model of Murray and Oster (1984) treats the epithelial sheet as a linear, isotropic, viscoelastic continuum, an approach which is justified as a reasonable first approximation in the absence of detailed knowledge of the mechanical properties of cytogel, and which is discussed from a rheological viewpoint by Elson (1988). Following wounding, the cytoskeleton undergoes rapid changes, on a time scale of a few minutes (Midwinter et al. 1992), reaching a new "quasi-equilibrium" state. Of course, this new state also changes over a time scale of a few hours, as healing proceeds. However, we do not consider here the processes occurring on this longer time scale; rather, we investigate the post-wounding quasi-equilibrium. In Murray and Oster's (1984) model and other related models (see Murray 1989), cellular contraction forces are controlled by the concentration of free calcium. Since we are only interested in an equilibrium state, chemical control is equivalent to an imposed spatial variation in parameter values; we neglect such effects, and assume that the mechanical properties of the cell sheet change only in response to the local stress and strain fields. These mechanical properties are determined largely by the transcellular network of actin filaments, which are linked at cell-cell adherens junctions (Pollard 1990). Our model addresses the equilibrium state of this network.

We take the stress tensor in the cell sheet to be

$$\underline{\underline{\sigma}} = \underbrace{G(E\underline{\underline{\varepsilon}} + \Gamma\nabla\cdot\underline{u}\,\underline{\underline{I}})}_{\substack{\text{elastic}\\ \text{stress}}} + \underbrace{\tau G\underline{\underline{I}}}_{\substack{\text{active}\\ \text{contraction}\\ \text{stress}}} \tag{1}$$

where $\underline{u}(\underline{r})$ is the displacement of the material point initially at $\underline{r}$, the strain tensor $\underline{\underline{\varepsilon}} = \frac{1}{2}(\nabla\underline{u} + \nabla\underline{u}^T)$, $G(\underline{r})$ is the density of intracellular actin filaments at the material point initially at $\underline{r}$, E and Γ are positive constants, and $\underline{\underline{I}}$ is the unit tensor. As

discussed below, the traction stress per filament, τ, is in general a function of the local compaction. The exertion of traction forces by fibroblasts has been extensively studied (see, for example, Harris 1982, Stopak and Harris 1982), and traction forces have been observed in a range of other cell types, including chick embryonic corneal epithelial cells (Mattey and Garrod 1984). The elasticity of the actin filament network arises from the extensive interpenetration of the long actin filaments, which tends to immobilize them (Janmey et al. 1988). In contrast to previous mechanical models of morphogenesis (Oster et al. 1983, Murray and Oster 1984, Oster 1984, Oster et al. 1985, Murray et al. 1988), we omit the viscous contribution in (1) since we are considering only the equilibrium state.

At equilibrium, these elastic and traction forces balance the elastic restoring forces that arise from attachment to the substratum. Following Murray and Oster (1984), we model these restoring forces by $\lambda G\underline{u}$, where the positive constant λ reflects the strength of the attachments. The term is proportional to G since most of the intracellular actin filaments terminate at, or close to, a region of adhesion to the substratum (Burridge et al. 1988); Hergott et al. (1989) and Wechezak et al. (1989) present direct experimental evidence for this proportionality.

Thus the equation to be solved for the new equilibrium configuration is

$$\nabla \cdot \underline{\underline{\sigma}} - \lambda G\underline{u} = \underline{0} \tag{2}$$

with $\underline{\underline{\sigma}}$ as in (1). We treat the cell sheet as infinite, which is a valid approximation provided the wound area is small compared to the whole sheet, and two-dimensional, since its thickness is about 10 μm, whereas a typical wound dimension is about 500 μm. Thus the boundary conditions are $\underline{u}(\infty) = \underline{0}$, and $\underline{\underline{\sigma}} \cdot \hat{\underline{n}} = \underline{0}$ at the free edge, where $\hat{\underline{n}}$ is the unit vector normal to this edge. Our approach in deriving (1), (2) and the boundary conditions assumes that in the pre-wounding state, $\underline{u} = \underline{0}$ everywhere. This is not an entirely trivial assumption in a developing embryo, but observations of the epithelial sheet prior to wounding indicate that, to a good approximation, the cell density is uniform and the substratum attachments are reforming sufficiently fast that the restoring forces exerted by them are negligible.

A crucial feature of the model (2) is the relationship between G and $\underline{u}$. In this paper we investigate whether the actin cable observed at the wound edge could be formed simply as a result of local compaction of the actin filament network. Specifically, we make the following key assumption:

> the response to wounding involves neither de novo actin polymerization, nor intracellular movement of intact actin filaments, so that the amount of filamentous actin in a given region of cytogel remains constant as that region is deformed.

There is a limited experimental evidence that this is the mechanism of cytoskeletal reorganization in some other systems (Chen 1981, Albrecht-Buehler 1987). The time scale over which the actin cable forms (a few minutes) is certainly consistent with this assumption, but does not exclude actin polymerization. For instance, on sudden exposure to a chemoattractant peptide, neutrophils form pseudopodia over their entire surface, and the proportion of intracellular actin that is polymerized rises from about 30% to about 60% in 20 seconds (Carson et al. 1986).

Thus, we assume that $G(1 - \Omega) = \kappa$, a spatially independent constant, where Ω is the fraction of its pre-wounding volume by which a small region of cytogel

contracts in the response to wounding. Substituting this into (2) gives the governing equation as

$$\nabla \cdot \left[\frac{\kappa}{1-\Omega} \{ E\underline{\underline{\varepsilon}} + \Gamma \nabla \cdot \underline{u}\underline{\underline{I}} + \tau \underline{\underline{I}} \} \right] - \frac{\lambda_\kappa}{1-\Omega} \underline{u} = \underline{0}. \tag{3}$$

It remains to consider the functional form of τ, the traction stress per filament. When a region of the actin filament network is compressed, the degree of filament overlap increases. Consequently additional myosin cross-bridges form between actin filaments (Oster and Odell 1984a), with a corresponding increase in the traction stress per filament. This is effectively a synergy phenomenon: actin filaments together exert a greater traction force than the sum of the traction forces they exert separately. We model this by taking τ to be an increasing function of the local compaction Ω, following previous mechanochemical models of epithelium (Oster 1984, Oster and Odell 1984a,b, Oster et al. 1985). Specifically, we take $\tau = \tau_0/(1-\beta\Omega)$. Thus a decrease in dilation at a point causes an increase in the traction stress at that point both because of an increase in the actin filament density at the point and because of an increase in the traction stress per filament. Intuitively, we expect the former effect to be larger than the latter, and thus we require that $0 < \beta < 1$. With this constraint, τ is bounded, since $\Omega < 1$ (a region cannot be compressed to a point).

To clarify the roles of the various model parameters, we nondimensionalize (3) by defining

$$\underline{r}^* = \underline{r}/L \qquad \underline{u}^* = \underline{u}/L \qquad E^* = E/\tau_0 \qquad \Gamma^* = \Gamma/\tau_0 \qquad \lambda^* = \lambda L^2/\tau_0$$

where * denotes a dimensionless quantity and L is a typical linear dimension of the wound. The available experimental data (for example Sato et al. 1987, Dennerll et al. 1988) is insufficient to determine any of E^*, Γ^*, λ^* or β. In the remainder of the paper we drop the asterisks for notational simplicity and use the superscript $^{\text{dim}}$ to denote the dimensional value corresponding to a given dimensionless parameter. Substituting these rescalings into (3) gives the dimensionless model equation as

$$\nabla \cdot \left[\frac{1}{1-\Omega} \left\{ E\underline{\underline{\varepsilon}} + \Gamma \nabla \cdot \underline{u}\underline{\underline{I}} + \frac{1}{1-\beta\Omega} \underline{\underline{I}} \right\} \right] - \frac{\lambda}{1-\Omega} \underline{u} = \underline{0}. \tag{4}$$

3 One-dimensional solutions

Solutions of the model in one spatial dimension are important for two reasons. Firstly, a study of the one-dimensional equations increases our mathematical understanding of the system, which can then be extended to the more biologically relevant two-dimensional equations. Secondly, the solutions may be applicable both to regions of square wounds away from the corners and to linear slash wounds.

In one spatial dimension, the dimensionless governing Eq. (4) is

$$\frac{d}{dx} \left[\frac{1}{1+u_x} \left\{ (E+\Gamma)u_x + \frac{1}{1+\beta u_x} \right\} \right] - \frac{\lambda}{1+u_x} u = 0 \tag{5}$$

with boundary conditions

$$(E+\Gamma)u_x + \frac{1}{1+\beta u_x} = 0 \quad \text{at } x = 0 \tag{6a}$$

$$u = 0 \quad \text{at } x = \infty. \tag{6b}$$

Here u_x denotes du/dx, and we take $x = 0$ to be the wound edge. Integrating this equation and using the boundary condition (6b) gives

$$\tfrac{1}{2}\lambda u^2 = P(u_x) \tag{7}$$

where if $\beta \neq 1$

$$P(u_x) = (E + \Gamma)[u_x - \log(1 + u_x)] + \frac{1}{1-\beta}\log(1 + u_x) - \frac{2-\beta}{\beta(1-\beta)}\log(1 + \beta u_x) - \frac{1}{\beta(1 + \beta u_x)} + \frac{1}{\beta}, \tag{8a}$$

and if $\beta = 1$

$$P(u_x) = (E + \Gamma)u_x - (E + \Gamma + 2)\log(1 + u_x) - \frac{2}{1 + u_x} + 2. \tag{8b}$$

The case $\beta = 1$ is not relevant biologically, but we will consider it briefly for mathematical completeness.

We write the boundary condition (6a) as

$$Q(u_x) \equiv (E + \Gamma)\beta u_x^2 + (E + \Gamma)u_x + 1 = 0. \tag{9}$$

When this has real roots for u_x, these are clearly negative. But from (8), $u_x = 0$ only if $u = 0$, and thus the boundary condition (6b) implies that solutions must be monotonically decreasing. We now prove that for $\beta > 0$, a solution exists if and only if

$$\hat{E} > \frac{1}{1-\beta} \quad \text{and} \quad 0 < \beta \leqslant 1/2$$
$$\text{or} \quad \hat{E} \geqslant 4\beta \quad \text{and} \quad \beta > 1/2,$$

and that this solution then satisfies the physical constraint $u_x > -1$ (a region cannot be compressed to a point). Here, and throughout the derivation of these conditions, we write $\hat{E} = (E + \Gamma)$ for notational simplicity.

Consider first the case $\beta < 1$. As discussed above, this is the case of interest biologically; we consider $\beta \geqslant 1$ later for mathematical completeness. The form of $P(u_x)$ on $-1 < u_x \leq 0$ depends on $\hat{E}$ and β. For $\hat{E} > 1/(1-\beta)$, $P(u_x) \to +\infty$ as $u_x \to -1^+$, while for $\hat{E} < 1/(1-\beta)$, $P(u_x) \to -\infty$ as $u_x \to -1^+$. When $\hat{E} = 1/(1-\beta)$,

$$P(-1) = \frac{-2\beta - (2-\beta)\log(1-\beta)}{\beta(1-\beta)} = \frac{2-\beta}{\beta(1-\beta)}\left[\frac{-2\beta}{2-\beta} - \log(1-\beta)\right].$$

This is strictly positive when $0 < \beta < 1$, since then $[(2-\beta)/(\beta(1-\beta))] > 0$, and also

$$\frac{d}{d\beta}\left[\frac{-2\beta}{2-\beta} - \log(1-\beta)\right] = \frac{\beta^2}{(2-\beta)^2(1-\beta)} > 0,$$

with $[-2\beta/(2-\beta) - \log(1-\beta)]\big|_{\beta=0} = 0$, so that $[-2\beta/(2-\beta) - \log(1-\beta)] > 0$ when $0 < \beta < 1$. Differentiating (8a) with respect to u_x gives

$$P'(u_x) = \frac{\hat{E}u_x}{1 + u_x} - \frac{\beta u_x}{(1 + \beta u_x)^2} - \frac{u_x}{(1 + u_x)(1 + \beta u_x)},$$

so that $P'(0) = 0$ and, differentiating again, $P''(0) = \hat{E} - (1 + \beta)$. Thus for small u_x, $P(u_x)$ has the same sign as $\hat{E} - (1 + \beta)$.

Apart from the root at $u_x = 0$,

$$P'(u_x) = 0 \Leftrightarrow \hat{E}(1+\beta u_x)^2 = \beta(1+u_x) + (1+\beta u_x)$$
$$\Leftrightarrow u_x = \frac{(1-\hat{E}) \pm \sqrt{\hat{E}\beta - \hat{E} + 1}}{\hat{E}\beta}.$$

These roots are real if and only if $\hat{E} \leqslant 1/(1-\beta)$. Then the larger root lies in $[-1, 0)$ if $\hat{E} > 1+\beta$, and is positive if $\hat{E} < 1+\beta$; the smaller (more negative) root is less than -1. For,

$$\frac{(1-\hat{E}) + \sqrt{\hat{E}\beta - \hat{E} + 1}}{\hat{E}\beta} < 0 \Leftrightarrow \sqrt{\hat{E}\beta - \hat{E} + 1} < \hat{E} - 1$$
$$\Leftrightarrow \hat{E} > 1 \quad \text{and} \quad \hat{E}\beta - \hat{E} + 1 < (\hat{E}-1)^2$$
$$\Leftrightarrow \hat{E} > 1 + \beta;$$

$$\frac{(1-\hat{E}) + \sqrt{\hat{E}\beta - \hat{E} + 1}}{\hat{E}\beta} > -1 \Leftrightarrow \sqrt{\hat{E}\beta - \hat{E} + 1} > -(\hat{E}\beta - \hat{E} + 1)$$

which is trivially satisfied provided $\hat{E} \neq 1/(1-\beta)$, in which case the root is equal to -1;

$$\frac{(1-\hat{E}) - \sqrt{\hat{E}\beta - \hat{E} + 1}}{\hat{E}\beta} < -1 \Leftrightarrow -\sqrt{\hat{E}\beta - \hat{E} + 1} < -(\hat{E}\beta - \hat{E} + 1)$$
$$\Leftrightarrow \hat{E}\beta - \hat{E} + 1 < 1,$$
since $\hat{E} \leqslant 1/(1-\beta)$
$$\Leftrightarrow \beta < 1.$$

Taking all these considerations into account, the form of $P(u_x)$ on $[-1, 0]$ as $\hat{E}$ and β vary is as shown in Fig. 1.

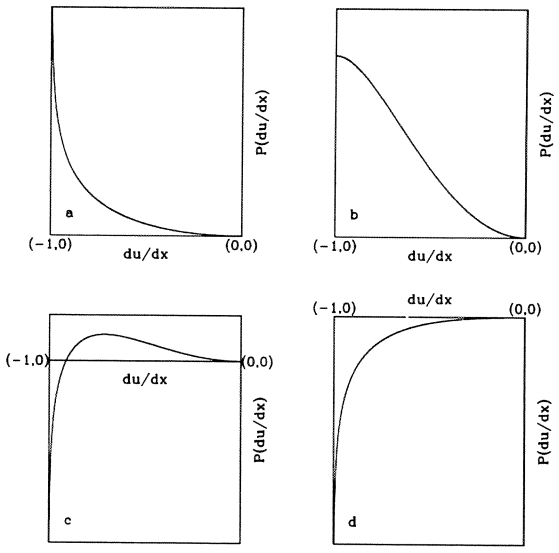

Fig. 1. The qualitative form of the function $P(u_x)$, given in (8a), as $\hat{E}$ and β vary with $\beta < 1$. (a) $\hat{E} > 1/(1-\beta)$; (b) $\hat{E} = 1/(1-\beta)$; (c) $(1+\beta) < \hat{E} < 1/(1-\beta)$; (d) $\hat{E} < (1+\beta)$

The roots $q_\pm$ of the boundary condition (9) are

$$q_\pm = \frac{-\hat{E} \pm \sqrt{\hat{E}^2 - 4\hat{E}\beta}}{2\hat{E}\beta}.$$

These are real if and only if $\hat{E} > 4\beta$, in which case they are both negative. Now $Q(0) = 1$ and $Q(-1) = \hat{E}(\beta - 1) + 1$. Thus if $\hat{E} > 1/(1-\beta)$, exactly one root of the quadratic Q lies in $(-1, 0)$, that is

$$q_+ \in (-1, 0) \quad \text{and} \quad q_- < -1 \quad \text{if } \hat{E} > \frac{1}{1-\beta}. \tag{10}$$

Conversely, if $4\beta < \hat{E} < 1/(1-\beta)$, both roots of Q lie in $(-1, 0)$ if $q_{\min} \in (-1, 0)$, and both roots are less than -1 if $q_{\min} < -1$. Here $q_{\min}$ is the value of u_x minimizing Q, and straightforward differentiation gives $q_{\min} = -1/2\beta$. Thus when $4\beta < \hat{E} < 1/(1-\beta)$,

$$-1 < q_+, q_- < 0 \quad \text{if } \beta > 1/2 \tag{11a}$$

$$q_+, q_- < -1 \quad \text{if } \beta < 1/2. \tag{11b}$$

We are now in a position to prove the conditions for the existence and uniqueness of solutions of (7) subject to (9) in the case $\beta < 1$. From (10) and the forms of $P(u_x)$ in Fig. 1, it is clear that if $\hat{E} > 1/(1-\beta)$ there is a unique monotonically decreasing solution of (7) subject to (9). For then $P(u_x)$ decreases monotonically from $+\infty$ to zero on $(-1, 0]$. Thus there is a 1–1 correspondence between $u \geqslant 0$ and $u_x \in (-1, 0]$, given by the governing equation (7), and moreover exactly one of the roots for u_x of the boundary conditions (9) lies in $(-1, 0)$.

In addition, if $1 + \beta < \hat{E} < 1/(1-\beta)$, there is a unique solution provided $\beta > 1/2$, $\hat{E} > 4\beta$ (so that $q_\pm$ are real) and $q_- < p_{\max} < q_+$; we prove below that the first two of these conditions together imply the third. Here $p_{\max}$ is the value of u_x at which P attains its maximum on $(-1, 0)$, that is

$$p_{\max} = \frac{(1-\hat{E}) + \sqrt{\hat{E}\beta - \hat{E} + 1}}{\hat{E}\beta}.$$

For then $P(u_x)$ decreases monotonically to zero on $[p_{\max}, 0]$. Thus there is a 1–1 correspondence between $u \in [0, P(p_{\max})]$ and $u_x \in [p_{\max}, 0]$, given by the governing Eq. (7). Moreover, exactly one of the roots for u_x of the boundary condition (9) lies in $(p_{\max}, 0)$. Note that $\beta > 1/2$ and $\hat{E} > 4\beta$ together imply that the condition $\hat{E} > 1 + \beta$ is satisfied. Moreover, these three conditions are necessary when $1 + \beta < \hat{E} < 1/(1-\beta)$, except for the case of $\hat{E} = 4\beta$. But then if $\beta > 1/2$, $p_{\max} = q_+ = q_- = -1/2\beta$, and thus there is a unique solution, while if $\beta < 1/2$, $q_+ = q_- = -1/2\beta < p_{\max}$, and thus there is no solution.

We now prove that $q_- < p_{\max} < q_+$ when $4\beta < \hat{E} < 1/(1-\beta)$ and $\beta > 1/2$. We have that

$$\begin{aligned}
q_- < p_{\max} &\Leftrightarrow -\sqrt{\hat{E}^2 - 4\hat{E}\beta} < 2 - \hat{E} + 2\sqrt{\hat{E}\beta - \hat{E} + 1} \\
&\Leftrightarrow \hat{E}^2 - 4\hat{E}\beta > [2 - \hat{E} + 2\sqrt{\hat{E}\beta - \hat{E} + 1}]^2 \\
&\quad \text{or } 2 - \hat{E} + 2\sqrt{\hat{E}\beta - \hat{E} + 1} > 0 \\
&\Leftrightarrow 2(\hat{E}\beta - \hat{E} + 1) < (\hat{E} - 2)\sqrt{\hat{E}\beta - \hat{E} + 1} \\
&\quad \text{or } 2\sqrt{\hat{E}\beta - \hat{E} + 1} > (\hat{E} - 2) \\
&\Leftrightarrow 2\sqrt{\hat{E}\beta - \hat{E} + 1} \neq (\hat{E} - 2) \\
&\Leftrightarrow \hat{E} \neq 4\beta
\end{aligned}$$

$$\begin{aligned}
\text{and } p_{\max} < q_+ &\Leftrightarrow 2 - \hat{E} + 2\sqrt{\hat{E}\beta - \hat{E} + 1} < \sqrt{\hat{E}^2 - 4\hat{E}\beta} \\
&\Leftrightarrow [2 - \hat{E} + 2\sqrt{\hat{E}\beta - \hat{E} + 1}]^2 < \hat{E}^2 - 4\hat{E}\beta \\
&\quad \text{or } 2 - \hat{E} + 2\sqrt{\hat{E}\beta - \hat{E} + 1} < 0 \\
&\Leftrightarrow 2(\hat{E}\beta - \hat{E} + 1) < (\hat{E} - 2)\sqrt{\hat{E}\beta - \hat{E} + 1} \\
&\quad \text{or } 2\sqrt{\hat{E}\beta - \hat{E} + 1} < (\hat{E} - 2) \\
&\Leftrightarrow 2\sqrt{\hat{E}\beta - \hat{E} + 1} < (\hat{E} - 2) \\
&\Leftrightarrow \hat{E} > 4\beta.
\end{aligned}$$

In these inequalities, we use the fact that $\hat{E} > 4\beta$ and $\beta > 1/2$ together imply that $\hat{E} > 2$.

Finally, for $\beta < 1$, we consider the outstanding case of $\hat{E} = 1/(1-\beta)$. Then $P(u_x)$ has the form shown in Fig. 1b: $P(-1)$ is finite and strictly positive, and $P'(-1) = 0$. But when $\hat{E} = 1/(1-\beta)$, the roots of Q are

$$q_+ = -1 \quad \text{and} \quad q_- = 1 - \frac{1}{\beta} < -1 \quad \text{if } \beta < 1/2$$

$$q_- = -1 \quad \text{and} \quad q_+ = 1 - \frac{1}{\beta} \in (-1, 0) \quad \text{if } \beta > 1/2.$$

Now $P'(-1) = 0$ in this case, and thus from (7), $u(0) > 0$ and $u_x(0) = -1$ together imply that $u_{xx}(0)$ is undefined, which is inadmissible since the original Eq. (5) is of second order. Thus when $\hat{E} = 1/(1-\beta)$, there is a solution, which is then unique and satisfies $u_x > -1$, if and only if $\beta > 1/2$.

For mathematical completeness, we now consider the case of $\beta \geqslant 1$. If $\beta = 1$, similar calculations to those above show that $P(u_x)$ has the qualitative form shown in Fig. 1c if $\hat{E} > 2$ and that shown in Fig. 1d if $\hat{E} < 2$. Also, the roots of Q are real if and only if $\hat{E} > 4$, in which case $-1 < q_{\min} < q_{\max} < q_{\max} < 0$. Thus there is a unique monotonically decreasing solution of (7) subject to (9) if and only if $\hat{E} > 4$.

If $\beta > 1$, the form of $P(u_x)$ is different. For then $P(u_x) \to -\infty$ as $u_x \to -(1/\beta)^+$. The qualitative form of $P(u_x)$ on $(-1/\beta, 0)$ depends on the sign of $P''(0) = \hat{E} - (1+\beta)$, and the two cases are shown in Fig. 2. Now $Q(-1/\beta) = 1 = Q(0)$, while $q_{\min} = -1/2\beta$. Thus, provided $\hat{E} > 4\beta$ so that Q has real roots, both the roots, q_+ and q_-, lie in $(-1/\beta, 0)$. Moreover, the inequalities $q_- < p_{\max} < q_+$ are still valid when $\hat{E} > 4\beta$. Thus when $\beta > 1$, there is a unique monotonically decreasing solution of (7) subject to (9) if and only if $\hat{E} \geqslant 4\beta$. (When $\hat{E} = 4\beta$, $q_- = q_+ = p_{\max} = -1/2\beta$, as for $1/2 < \beta < 1$).

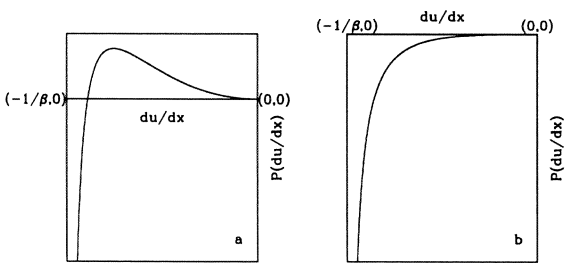

Fig. 2. The qualitative form of the function $P(u_x)$, given in (8a), as $\hat{E}$ and β vary with $\beta > 1$.
(a) $\hat{E} > 1 + \beta$; (b) $\hat{E} < 1 + \beta$

We have shown that in one spatial dimension, a solution of the model Eq. (4) subject to the biologically appropriate boundary conditions (6) exists if and only if

$$\beta < 1 - 1/\hat{E}, \qquad 1 \leqslant \hat{E} \leqslant 2$$
$$\beta \leqslant \hat{E}/4, \qquad \hat{E} > 2,$$

and that this solution is then unique, monotonically decreasing, and satisfies the physical constraint $u_x > -1$. Our interpretation of β as a parameter that increases gradually with time (see Sect. 5, below) means that β will always be sufficiently small for a steady state solution to exist. To capture the experimentally observed phenomenon of the actin cable at the wound edge, we require that $G(x)$ has a sharp peak at $x = 0$. Now $G(x) = 1/(1 + u_x)$, and we therefore require $u_x(0)$ close to -1. Our analysis shows that this will be satisfied provided $1 \leqslant \hat{E} \leqslant 2$, with β close to $1 - 1/\hat{E}$. We will discuss the biological interpretation of this result below.

4 Two-dimensional radially symmetric solutions

We now consider solutions of the model equations in a radially symmetric cylindrical geometry, corresponding to a circular wound. Then $\Omega = 1 - (1 + u/r)(1 + u')$, so that Eq. (4) simplifies to

$$u'' = \frac{1}{(E + \tau_2)(r + u) + \Gamma(r - u^2/4)} \cdot \left\{ \lambda r u \left[1 + u' + \frac{u}{r} + \frac{uu'}{r} \right] - \left(u' - \frac{u}{r} \right) \left[E\left(1 + \frac{u}{r} - u'^2 + \frac{uu'}{r} \right) + \Gamma(1 - u'^2) + \tau_2(1 + u') \right] \right\} \quad (12)$$

where r is the radial coordinate, prime denotes d/dr, and

$$\tau_2 = -\left[\frac{1}{1 + \beta(u' + u/r + uu'/r)} + \frac{\beta(1 + u' + u/r + uu'/r)}{\{1 + \beta(u' + u/r + uu'/r)\}^2} \right].$$

We take the length scale L used in the nondimensionalization to be the wound radius, so that the boundary conditions are

$$Eu' + \Gamma(u' + u) + \frac{1}{1 + \beta(u' + u + uu')} = 0 \quad \text{at } r = 1 \quad (13a)$$

$$u = 0 \quad \text{at } r = \infty. \quad (13b)$$

Since there are only four parameters, a detailed numerical investigation of this highly nonlinear equation was possible; a simplified version of the equation has previously been studied analytically using singular perturbation theory (Sherratt 1991). As in the one-dimensional case, this numerical study revealed a unique, monotonically decreasing solution provided $\beta < \beta_{\text{crit}}$, with β_{crit} depending on E, Γ, and, in this new geometry, on λ. Moreover, for sufficiently small E and Γ, as $\beta \to \beta_{\text{crit}}$, $u'(1) \to -1$ and thus the filamentous actin density $G(r) = 1/[(1 + u/r)(1 + u')]$ develops a sharp peak at the wound edge, which is sufficiently localized that it reflects the phenomenon of the actin cable. A typical solution for β close to β_{crit} is illustrated in Fig. 3.

We have been unable to derive an exact analytical expression for β_{crit}, but for $E + \Gamma \leqslant 2$, we have obtained an analytical approximation that is valid for large

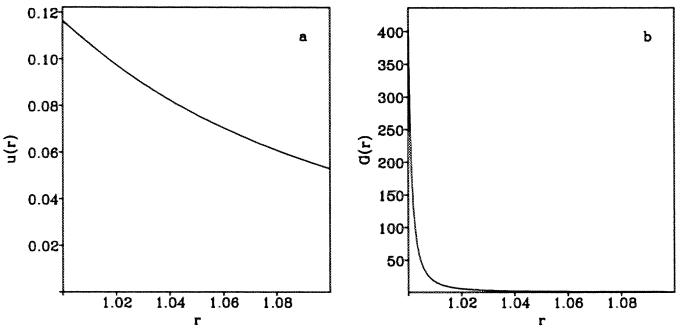

Fig. 3. (a) A typical solution of (12) subject to (13) for β close to β_{crit}. (b) The corresponding dimensionless actin filament density $G(r)$. The parameter values are $\lambda = 3.0$, $E = 0.5$, $\Gamma = 0.8$ and $\beta = 0.17$; for these values of E, Γ and λ, we estimate numerically that $\beta_{\text{crit}} \approx 0.1989$. The equation is solved numerically using a finite difference scheme and Newton's method, with deferred correction and continuation in β (Pereyra, 1979). For a typical wound radius of 500 μm, the dimensionless cell length is 0.02. This solution therefore captures the experimental observation of a cable of filamentous actin at the wound edge, localized within the leading row of basal cells

λ. Recall that the nondimensionalization we have used implies that the dimensionless parameter λ is given by ΛR^2, where R is the dimensional wound radius, and the dimensional quantity Λ is the ratio of the dimensional parameters λ^{dim} and τ_0. But in the limit $R \to \infty$, the radially symmetric geometry approaches the one-dimensional geometry, in which the critical upper limit β is $[1 - 1/(E + \Gamma)]$. Thus as $\lambda \to \infty$, $\beta_{\text{crit}} = 1/(E + \Gamma) + o(1)$.

In the one-dimensional equations, $u_x|_{\text{w.e.}} \to -1$ as $\beta \to 1 - 1/(E + \Gamma)$, where '$|_{\text{w.e.}}$' denotes 'at the wound edge'. Equation (7) therefore implies that in one dimension, the displacement at the wound edge in this limiting case is given by

$$u_{\text{w.e.}} = \sqrt{2P(-1)/\lambda}\,|_{\beta = 1 - 1/(E+\Gamma)}$$
$$= \left[\frac{2}{\lambda}\left\{\frac{(E+\Gamma)(E+\Gamma+1)}{(E+\Gamma-1)}\log(E+\Gamma) - 2(E+\Gamma)\right\}\right]^{1/2}.$$

Now in one dimension, $\lambda = \Lambda L^2$, where L is the length scale used in the nondimensionalization. Thus the limiting dimensional value of the displacement at the wound edge in the one-dimensional geometry is

$$u(0) \cdot L = \left[\frac{2}{\Lambda}\left\{\frac{(E+\Gamma)(E+\Gamma+1)}{(E+\Gamma-1)}\log(E+\Gamma) - 2(E+\Gamma)\right\}\right]^{1/2}. \qquad (14)$$

Returning to the two-dimensional radially symmetric geometry, the singularity as $\beta \to \beta_{\text{crit}}$ arises in this case because $du/dr(1) \to -1$. Therefore the boundary condition (13a) implies that in this critical case

$$u(1) = \frac{1}{\Gamma}\left(E + \Gamma - \frac{1}{1 - \beta_{\text{crit}}}\right).$$

Now in the limit as the wound radius $R \to \infty$, the dimensional displacement at the wound edge in the two-dimensional radially symmetric geometry must tend to the dimensional displacement at the wound edge in the one-dimensional

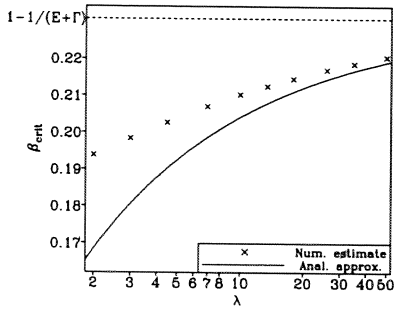

Fig. 4. The analytical approximation (15) of β_{crit} compared to numerical estimates for a range of values of λ. The other parameter values are $E = 0.5$ and $\Gamma = 0.8$. For clarity, λ is plotted on a logarithmic scale

geometry. (Of course, the dimensionless displacement tends to zero in the former case.) Thus as $R \to \infty$,

$$\frac{R}{\Gamma}\left(E+\Gamma-\frac{1}{1-\beta_{\text{crit}}}\right) = \left[\frac{2}{\lambda}\left\{\frac{(E+\Gamma)(E+\Gamma+1)}{(E+\Gamma-1)}\log(E+\Gamma)-2(E+\Gamma)\right\}\right]^{1/2}+o(1).$$

Dividing by R gives

$$\frac{1}{\Gamma}\left(E+\Gamma-\frac{1}{1-\beta_{\text{crit}}}\right) = \left[\frac{2}{\lambda}\left\{\frac{(E+\Gamma)(E+\Gamma+1)}{(E+\Gamma-1)}\log(E+\Gamma)-2(E+\Gamma)\right\}\right]^{1/2}+o(\lambda^{-1/2})$$

as $\lambda \to \infty$, that is

$$\beta_{\text{crit}} = 1-\left\{E+\Gamma-\left[\frac{2\Gamma^2}{\lambda}\left\{\frac{(E+\Gamma)(E+\Gamma+1)}{(E+\Gamma-1)}\log(E+\Gamma)-2(E+\Gamma)\right\}\right]^{1/2}\right\}^{-1} + o(\lambda^{-1/2}). \tag{15}$$

as $\lambda \to \infty$. This approximation is illustrated in Fig. 4.

5 Biological interpretation of β

An important issue raised by the model is the biological interpretation of the result that solutions only reflect the phenomenon of the actin cable when β is close to β_{crit}. Such an interpretation emerged when we examined the biological literature on the relative rates of intracellular rearrangement of myosin and filamentous actin. Experimental studies of actin filament reorganization in response to micromanipulation have shown that this process occurs on a time scale of a few seconds (Kolega 1986, Chen 1981). In contrast, intracellular movement of myosin is considerably slower, with a time scale of several minutes (Nachmias et al. 1989, McKenna et al. 1989). In a particularly relevant experiment, DeBiasio et al. (1988) studied the actin and myosin content of cellular protrusions in migrating fibroblasts by microinjecting fluorescent derivatives. They found that while actin was immediately present in these protrusions, in fact at somewhat elevated levels, myosin only became detectable after 1–2 minutes.

Thus experimental evidence suggests that the reorganization of actin filaments in response to wounding might be considerably quicker than the

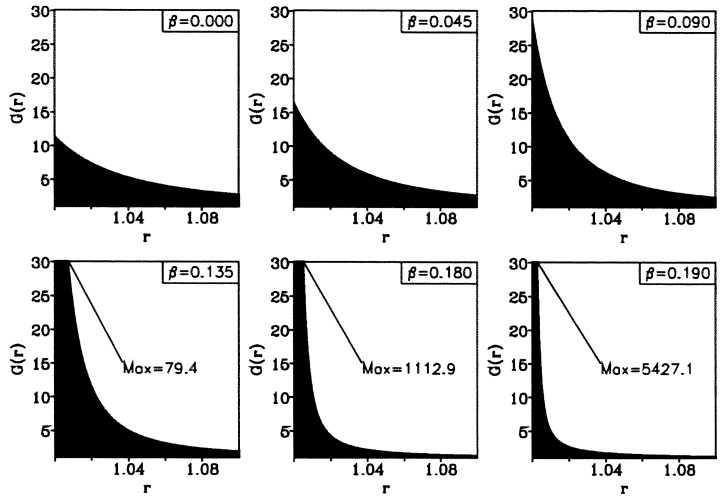

Fig. 5. The actin filament density $G(r)$ plotted against $u(r) + r$, the post-wounding radial position of the material point initially at radius r, for a range of values of β. The other parameter values are $E = 0.5$, $\Gamma = 0.8$, $\lambda = 3.0$; for these values, we estimate numerically that $\beta_{crit} \approx 0.1989$. When $G(1)$ is greater than the upper limit of the vertical axis, its value is indicated. Since we are interpreting β as a parameter whose value increases gradually with time, we can regard this figure as a time sequence of actin filament densities during the first few minutes after wounding

corresponding reorganization of intracellular myosin. Recalling that the parameter β reflects the extent of myosin cross-bridging between actin filaments, we can think of β as a parameter whose value increases gradually with time. With this interpretation, we can regard the variation in the model solutions with increasing β as the time evolution of epidermal displacements during the first few minutes after wounding. The corresponding sequence of actin filament densities for a circular wound is illustrated in Fig. 5. As intracellular myosin is reorganized, the aggregation of filamentous actin at the wound edge increases, to an extent that corresponds to the actin cable observed experimentally. The parameter β is of course prevented from reaching β_{crit} by physical constraints on the packing of actin filaments, which are not included in our model. We should, however, stress that this interpretation of β is at best heuristic; full theoretical investigation of the role of myosin in the formation of the actin cable would require new detailed modelling of actomyosin interaction in non-muscle cells.

6 Conclusions

We have modified the mechanochemical model of Murray and Oster (1984) to investigate the post-wounding quasi-equilibrium of embryonic epidermis. Analysis of the model in both one-dimensional and radially symmetric two-dimensional geometries has shown that the model solutions can reflect the experimentally observed cable of filamentous actin at the wound edge, provided the parameter β is close to a critical upper limit, which depends on the other parameters in a way we have investigated analytically. We have also suggested a possible interpretation of this limit in terms of intracellular reorganization of

actin and myosin. In this paper we have focussed on the formation of the actin cable as a response to wounding. A second quantifiable aspect of the experimental observations is the retraction of the wound edge after injury. In a separate publication (Sherratt and Lewis 1992), we will show that the model solutions can only reflect this second aspect of the experimental results when the model is modified to incorporate stress-induced alignment of actin filaments. From the present study, we conclude that the actin cable observed at the edge of embryonic epidermal wounds (Martin and Lewis 1991, 1992) could form simply as a result of local compaction of the actin filament network, without either intracellular movement of intact actin filaments or de novo actin polymerization.

Acknowledgements. I would like to thank Professor J. D. Murray (Department of Applied Mathematics, University of Washington) and Dr. Philip Maini (Centre for Mathematical Biology, Oxford) for their invaluable help and inspiration. I am also very grateful to my biological collaborators Dr. Julian Lewis (ICRF, Oxford) and Dr. Paul Martin (Dept. of Human Anatomy, University of Oxford) for our many fascinating discussions. This research was funded in part by a graduate studentship from the Science and Engineering Research Council of Great Britain and in part by a Junior Research Fellowship at Merton College, Oxford.

References

Albrecht-Buehler, G.: Role of cortical tension in fibroblast shape and movement. Cell Motil. **7**, 54–67 (1987)

Burridge, K., Fath, K., Kelly, T., Nuckolls, G., Turner, C.: Focal adhesions: transmembrane junctions between the extracellular matrix and the cytoskeleton. Ann. Rev. Cell Biol. **4**, 487–525 (1988)

Carson, M., Weber, A., Zigmond, S. H.: An actin-nucleating activity in polymorphonuclear leukocytes is modulated by chemotactic peptides. J. Cell Biol. **103**, 2707–2714 (1986)

Chen, W.: Mechanism of retraction of the trailing edge during fibroblast movement. J. Cell Biol. **90**, 187–200 (1981)

Clark, R. A. F.: Wound repair. Curr. Op. Cell Biol. **1**, 1000–1008 (1989)

DeBiasio, R. L., Wang, L. L., Fisher, G. W., Taylor, D. L.: The dynamic distribution of fluorescent analogues of actin and myosin in protrusions at the leading edge of migrating Swiss 3T3 fibroblasts. J. Cell Biol. **107**, 2631–2645 (1988)

Dennerll, T. J., Joshi, H. C., Steel, V. L., Buxbaum, R. E., Heidemann, S. R.: Tension and compression in the cytoskeleton of PC-12 neurites. II. Quantitative measurements. J. Cell Biol. **107**, 665–674 (1988)

Elson, E. L.: Cellular mechanics as an indicator of cytoskeletal structure and function. Ann. Rev. Biophys. Biophys. Chem. **17**, 397–430 (1988)

Harris, A. K.: Traction, and its relations to contraction in tissue cell locomotion. In: Bellairs, R., Curtis, A., Dunn, G. (eds.) Cell behaviour, pp. 109–134. Cambridge: Cambridge University Press 1982

Hergott, G. J., Sandig, M., Kalnins, V. I.: Cytoskeletal organisation of migrating retinal pigment epithelial cells during wound healing in organ culture. Cell Motil. **13**, 83–93 (1989)

Janmey, P. A., Hvidt, S., Peetermans J., Lamb, J., Ferry, J. D., Stossel, T. P.: Viscoelasticity of F-actin and F-actin/gelsolin complexes. Biochem. **27**, 8218–8227 (1988)

Kolega, J.: Effects of mechanical tension on protrusive activity and microfilament and intermediate filament organization in an epidermal epithelium moving in culture. J. Cell Biol **102**, 1400–1411 (1986)

Martin, P., Lewis, J.: The mechanics of embryonic skin wound healing-limb bud lesions in mouse and chick embryos. In: Adzick, N. S., Longaker, M. T. (eds.) Fetal wound healing: a paradigm of tissue repair, pp. 265–279. New York: Elsevier 1991

Martin, P., Lewis, J.: Actin cables and epidermal movement in embryonic wound healing. Nature **360**, 179–183 (1992)

Mattey, D. L., Garrod, D. R.: Organization of extracellular matrix by chick embryonic corneal epithelial cells in culture and the role of fibronectin in adhesion. J. Cell Sci. **67**, 171–188 (1984)
McKenna, N. M., Wang, Y. L., Konkel, M. E.: Formation and movement of myosin-containing structures in living fibroblasts. J. Cell Biol. **109**, 1163–1172 (1989)
Midwinter, K., McCluskey, J., Martin, P.: Healing of slash lesions to the embryonic chick limb bud (submitted, 1992)
Murray, J. D.: Mathematical biology. Berlin Heidelberg New York: Springer 1989
Murray, J. D., Maini, P. K., Tranquillo, R. T.: Mechanochemical models for generating biological pattern and form in development. Phys. Rep. **171**, 59–84 (1988)
Murray, J. D., Oster, G. F.: Generation of biological pattern and form. IMA J. Math. Appl. Med. Biol. **1**, 51–75 (1984)
Nachmias, V. T., Fukui, Y., Spudich, J. A.: Chemoattractant-elicited translocation of myosin in motile *Dictyostelium*. Cell Motil **13**, 158–169 (1989)
Odell, G. M., Oster, G., Alberch, P., Burnside, B.: The mechanical basis of morphogenesis. Devel. Biol. **85**, 446–462 (1981)
Oster, G. F.: On the crawling of cells. J. Embryol. Exp. Morphol. **83** Suppl., 329–364 (1984)
Oster, G. F., Odell, G. M.: Mechanics of cytogels. I. Oscillations in *Physarum*. Cell Motil. **4**, 469–503 (1984a)
Oster, G. F., Odell, G. M.: The mechanochemistry of cytogels. Physica **12D**, 333–350 (1984b)
Oster, G. F., Murray, J. D., Harris, A. K.: Mechanical aspects of mesenchymal morphogenesis. J. Embryol. Exp. Morphol. **78**, 83–125 (1983)
Oster, G. F., Murray, J. D., Odell, G. M.: The formation of microvilli. In: Edelman, G. M. (ed.) Molecular determinants of animal form, pp. 365–384. New York: Alan R. Liss 1985
Pereyra, V.: PASVA3: an adaptive finite-difference fortran program for first order nonlinear ordinary boundary problems. In: Childs, B., Scott, M., Daniel, J. W., Denman, E., Nelson, P. (eds.) Codes for boundary value problems in ordinary differential equations (Lect. Notes Comput. Sci., vol. 76) Berlin Heidelberg New York: Springer 1979
Pollard, T. D.: Actin. Curr. Op. Cell Biol. **2**, 33–40 (1990)
Sato, M., Schwarz, W. H., Pollard, T. D.: Dependence of the mechanical properties of actin/α-actinin gels on deformation rate. Nature **325**, 828–830 (1987)
Sherratt, J. A.: A perturbation problem arising from a mechanical model for epithelial morphogenesis. IMA J. Appl. Math. **47**, 147–162 (1991)
Sherratt, J. A., Lewis, J.: Stress-induced alignment of actin filaments and the mechanics of cytogel. Bull. Math. Biol. **55**, 637–654 (1993)
Sherratt, J. A., Murray, J. D.: Mathematical analysis of a basic model for epidermal wound healing. J. Math. Biol. **29**, 389–404 (1991)
Sherratt, J. A., Murray, J. D.: Epidermal wound healing: a theoretical approach. Comments Theor. Biol. **2**, 315–333 (1992)
Stenn, K. S., De Palma, L.: Re-epithelialization. In: Clark, R. A. F., Henson, P. M. (eds.) The molecular and cellular biology of wound repair, pp. 321–335. New York: Plenum 1988
Stopak, D., Harris, A. K.: Connective tissue morphogenesis by fibroblast traction. I. Tissue culture observations. Dev. Biol. **90**, 383–398 (1982)
Wechezak, A. R., Wight, T. N., Viggers, R. F., Sauvage, L. R.: Endothelial adherence under shear stress is dependent upon microfilament reorganisation. J. Cell. Physiol. **139**, 136–146 (1989)
Winter, G. D.: Formation of the scab and the rate of epithelialization of superficial wounds in the skin of the young domestic pig. Nature **193**, 293–294 (1962)

Note added in proof

Since the acceptance of this paper, W. M. Bement et al. (J. Cell Biol. **121**: 565–578, 1993) have demonstrated the healing of wounds via an actin cable in Caco-2 epithelial cell monolayers in vitro. As predicted by the model presented here, they have shown that the densities of filamentous actin and myosin-II at the wound edge increase in parallel following wounding. This does not prove that the formation of the actin cable is dependent on the corresponding aggregation of myosin, but it is an important confirmation of our modelling results.